Breaking the *C. elegans* invasion/proliferation dichotomy

Michael A. Q. Martinez[1], Chris Z. Zhao[1], Frances E. Q. Moore[1], Callista Yee[2], Wan Zhang[1], Kang Shen[2], Benjamin L. Martin[1], David Q. Matus[1]

[1]Department of Biochemistry and Cell Biology, Stony Brook University, Stony Brook, NY 11794, USA.

[2]Howard Hughes Medical Institute, Department of Biology, Stanford University, Stanford, CA 94305, USA.

*Author for correspondence (david.matus@stonybrook.edu)

KEY WORDS: *C. elegans*, invasion, proliferation, dichotomy, CKI-1

ABSTRACT

The acquisition of the post-mitotic state is crucial for the execution of many terminally differentiated cell behaviors during organismal development. However, the mechanisms that maintain the post-mitotic state in this context remain poorly understood. To gain insight into these mechanisms, we used the genetically and visually accessible model of *C. elegans* anchor cell (AC) invasion into the vulval epithelium. The AC is a terminally differentiated uterine cell that must exit the cell cycle and enter a post-mitotic to initiate contact between the uterus and vulva through a cell invasion event. Here, we set out to identify the negative cell cycle regulators that maintain the AC in a post-mitotic, invasive state. Although our findings revealed a critical role for CKI-1 ($p21^{CIP1}$/$p27^{KIP1}$) in maintaining the post-mitotic state of the AC, loss of CKI-1 alone or in combination with other negative cell cycle regulators—including CKI-2 ($p21^{CIP1}$/$p27^{KIP1}$), LIN-35 (pRb/p107/p130), FZR-1 (Cdh1/Hct1), and LIN-23 (β-TrCP)—resulted in proliferating ACs that retained their invasive abilities. Upon examination of the gene regulatory network controlling AC invasion, we determined that proliferating, invasive ACs maintain pro-invasive gene expression. We therefore report that maintenance of the post-mitotic state is not necessary for AC invasion, breaking the previously established *C. elegans* invasion/proliferation dichotomy.

INTRODUCTION

The proper timing and coordination of terminal differentiation is critical for organismal development. In many cases, terminal differentiation requires cells to exit the cell cycle and enter a post-mitotic state (Soufi and Dalton, 2016). The general model for how terminally differentiated cells exit the cell cycle involves the repression of cyclin/CDK activity by negative cell cycle regulators such as CDK inhibitors (CKIs), retinoblastoma (Rb) family members, and E3 ubiquitin ligase complexes, including the anaphase-promoting complex/cyclosome (APC/C) and the Skp-Cullin-F-box protein (SCF) complex (Buttitta and Edgar, 2007; Ruijtenberg and van den Heuvel, 2016). Despite this generally accepted model, the mechanisms by which terminally differentiated cells maintain their post-mitotic state remain unclear.

Exit from the cell cycle following terminal differentiation is considered essential for the execution of specialized cell behaviors. According to the “go versus grow” dichotomy, a mutually exclusive relationship exists between these cell behaviors and cell proliferation (Kohrman and Matus, 2017). However, accumulating evidence has challenged this dichotomy in both development and cancer. For instance, in the developing mouse retina, genetic ablation of Rb paralogs leads to fully differentiated neurons that retain their ability to form neurites and synapses while proliferating (Ajioka et al., 2007). Similar results have been observed in mouse inner ear hair cells following loss of Rb (Sage et al., 2005). Furthermore, recent evidence from two-dimensional and three-dimensional *in vitro* assays using skin cancer cells found that these cells can simultaneously invade and proliferate (Haass et al., 2014; Vittadello et al., 2020).

Here, we used *C. elegans* anchor cell (AC) invasion as a genetically dissectible *in vivo* model of developmental cell invasion. Since the AC must exit the cell cycle and enter a post-mitotic state upon invasive differentiation (Deng et al., 2020; Matus et al., 2015; Medwig-Kinney et al., 2020; Smith et al., 2022), we aimed to identify the negative regulators of the AC cell cycle that maintain the post-mitotic state. While our findings reveal a critical role for the CDK inhibitor CKI-1 ($p21^{CIP1}$/$p27^{KIP1}$) in maintaining the post-mitotic state of the AC, loss of CKI-1 alone or in combination with other negative cell cycle regulators resulted in proliferating ACs that retained their invasive abilities. Using two reporters of the gene regulatory network that controls AC invasion, we show that proliferating, invasive ACs maintain pro-invasive gene expression. Thus, our work demonstrates that maintenance of the post-mitotic state is not required for AC invasion, breaking the invasion/proliferation dichotomy in *C. elegans*.

RESULTS AND DISCUSSION

Background

The *C. elegans* egg-laying system requires a direct connection between the uterus and the vulva. In the mid-L3 larval stage, a terminally differentiated post-mitotic uterine cell, called the anchor cell (AC), initiates the uterine-vulval connection by breaching the basement membrane (BM) that separates these tissues (Sherwood and Sternberg, 2003) (Fig. 1A, left). AC invasion occurs in synchrony with the divisions of P6.p, the underlying 1º-fated vulval precursor cell (VPC). By the P6.p 4-cell stage, BM dissolution is complete (Sherwood and Sternberg, 2003). Robust control of the AC cell cycle appears to be required for invasive differentiation, as loss of the post-mitotic state results in a complete loss of invasive capacity (Matus et al., 2015) (Fig. 1A, right). The SWI/SNF chromatin remodeling complex, specifically the evolutionarily conserved BAF assembly, along with three conserved transcription factors—EGL-43 (EVI1), HLH-2 (E/Daughterless), and NHR-67 (TLX/Tailless)—have all been implicated in the regulation of AC invasion because of their critical role in maintaining the post-mitotic state (Deng et al., 2020; Matus et al., 2015; Medwig-Kinney et al., 2020; Smith et al., 2022). However, the direct negative regulators of the AC cell cycle are largely unknown.

Uterine-specific depletion of CKI-1 rarely causes AC proliferation

In a genetic background where only the uterine cells are sensitive to RNAi (Hagedorn et al., 2009), loss of either EGL-43 or NHR-67 leads to AC proliferation without BM invasion in over 60% of animals (Matus et al., 2015; Medwig-Kinney et al., 2020). Conversely, uterine-specific RNAi-mediated depletion of CKI-1 ($p21^{CIP1}$/$p27^{KIP1}$), a canonical negative regulator of the *C. elegans* cell cycle (Feng et al., 1999; Fukuyama et al., 2003; Hong et al., 1998), rarely results in this phenotype, occurring in about 3% of animals (Matus et al., 2015).

In an attempt to increase the penetrance of the proliferative AC phenotype (≥2 AC), we first built a new RNAi construct for *cki-1* using the highly efficient RNAi vector, T444T (Sturm et al., 2018). Unlike the standard RNAi vector, L4440 (Timmons and Fire, 1998), T444T includes a pair of T7 terminator sequences to prevent transcription of the vector backbone. We then tested the T444T-based *cki-1(RNAi)* construct in a uterine-specific RNAi strain (*rrf-3(pk1426); rde-*

103 *1(ne219); fos-1ap::rde-1*) with fluorescent reporters to visualize the AC cell membrane and BM.
104 Though 5% of animals exposed to this construct had ≥2 ACs (Fig. S1A), this result only
105 represents a 2% increase in the proliferative AC phenotype when compared to the original *cki-*
106 *1(RNAi)* experiment (Matus et al., 2015). In each of these animals, BM invasion was observed.
107 This finding could be attributed to either a late RNAi effect or reestablishment of the post-mitotic,
108 invasive state following AC proliferation. Alternatively, this result raises the intriguing possibility
109 that ACs can simultaneously invade and proliferate, which we explore in the subsections below.
110
111 **Systemic depletion of CKI-1 causes a moderate increase in AC proliferation**
112
113 To better visualize the dichotomy between AC invasion and proliferation, we generated a strain
114 for three-color imaging of the AC, cell cycle, and BM (Fig. 1A-C). Specifically, this strain
115 contains an endogenous transcriptional reporter of *lag*-2 (*Delta*), LAG-
116 2::P2A::H2B::mTurquoise2, to mark the AC nucleus (Medwig-Kinney et al., 2022), a ubiquitous
117 CDK activity sensor, DHB::2xmKate2, to visualize and quantify cell cycle state (Adikes et al.,
118 2020), and an endogenous translational reporter of *lam-2*, LAM-2::mNeonGreen, to label
119 laminin, a core BM component (Jayadev et al., 2019). Conveniently, the histone-based *lag-2*
120 transcriptional reporter also functions as a P6.p lineage tracker, facilitating the developmental
121 staging of AC invasion (Fig. 1A,C). The CDK activity sensor is a fluorescent fragment of human
122 DNA helicase B (DHB), which is predominantly nuclear in post-mitotic cells, such as the wild-
123 type AC, and becomes increasingly cytoplasmic in proliferating cells as they progress through
124 the cell cycle (Fig. 1B,C). Thus, the ratio cytoplasmic-to-nuclear of DHB fluorescence provides a
125 visual and quantitative readout of CDK activity, and more generally, cell cycle progression
126 (Adikes et al., 2020; Martinez and Matus, 2022; Spencer et al., 2013; van Rijnberk et al., 2017).
127
128 With the three-color imaging strain at our disposal, we first wanted to determine the penetrance
129 of the proliferative AC phenotype following RNAi-mediated depletion of CKI-1 in a wild-type
130 background. Unexpectedly, 100% of *control(RNAi)* and *cki-1(RNAi)* animals showed a post-
131 mitotic, invasive AC (Fig. S1B,C; Table 1). We next introduced the *rrf-3(pk1426)* null allele
132 (Simmer et al., 2002), which on its own confers RNAi hypersensitivity in many somatic tissues,
133 including the uterus (Matus et al., 2010). While nearly all *rrf-3(pk1426); control(RNAi)* animals
134 contained a post-mitotic, invasive AC (Fig. 1D,E), there was one animal where a BM gap was
135 not observed below a post-mitotic AC (Table 1). In comparison, 24% of *rrf-3(pk1426); cki-*
136 *1(RNAi)* animals possessed ≥2 ACs, which correlated with a significant increase in AC-specific

137 CDK activity when compared to *rrf-3(pk1426); control(RNAi)* animals (0.25 ± 0.06 (n = 30) vs.
138 0.73 ± 0.56 (n = 55)). In almost half of those animals with ≥2 ACs, BM invasion was observed
139 (Table 1). Taken together, these data demonstrate that systemic depletion of CKI-1 enhances
140 the penetrance of the proliferative AC phenotype.
141
142 Unfortunately, we were unable to assess the effect of the *cki-1(gk132)* null allele on AC
143 proliferation (The *C. elegans* Deletion Mutant Consortium, 2012), as it leads to embryonic
144 lethality in 100% of homozygotes (Buck et al., 2009) (Fig. S2A). Instead, we crossed the *cdc-*
145 *14(he141)* null allele into the three-color imaging strain (Saito et al., 2004). *cdc-14* encodes a
146 dual-specificity phosphatase that positively regulates CKI-1 activity in a number of larval tissues
147 (Clayton et al., 2008; Roy et al., 2011; Roy et al., 2014; Saito et al., 2004), likely by preventing
148 its phosphorylation-dependent degradation (Saito et al., 2004). Nonetheless, 100% of *cdc-*
149 *14(he141)* animals had a post-mitotic, invasive AC, even in the presence of *cki-1(RNAi)* (Fig.
150 S2B,C; Table 1), suggesting that CDC-14 is not a regulator of CKI-1 in the AC or that its
151 function is redundant with that of another phosphatase.
152
153 In the following subsection, we introduce viable null or hypomorphic alleles that impact other
154 negative regulators of the cell cycle (*cki-2*, *lin-35*, *fzr-1*, and *lin-23*) to determine their role in
155 maintaining the post-mitotic state of the AC.
156
157 **CKI-1 is critical for maintaining the post-mitotic state of the AC**
158
159 Only a handful of factors negatively regulate the somatic cell cycle during *C. elegans* larval
160 development (Kipreos and van den Heuvel, 2019). These include the CDK inhibitors CKI-1 and
161 CKI-2 ($p21^{CIP1}$/$p27^{KIP1}$) (Buck et al., 2009; Hong et al., 1998), the sole Rb family member LIN-35
162 (pRb/p107/p130) (Boxem and van den Heuvel, 2001; Boxem and van den Heuvel, 2002), the
163 APC/C co-activator FZR-1 (Cdh1/Hct1) (Fay et al., 2002), and the F-box/WD-repeat protein LIN-
164 23 (β-TrCP) (Kipreos et al., 1996; Kipreos et al., 2000; Nayak et al., 2002). Although they all
165 ensure normal cell cycle exit either generally (CKI-1 and LIN-23), redundantly (LIN-35 and FZR-
166 1), or tissue specifically (CKI-2), their role in maintaining the post-mitotic state is poorly
167 understood.
168
169 To determine their role in the AC, we generated four separate three-color imaging strains. Three
170 of these strains include putative null alleles, i.e., *cki-2(ok2105)*, *lin-35(n745)*, or *lin-23(e1883)*

171 (Kipreos et al., 2000; Lu and Horvitz, 1998; The *C. elegans* Deletion Mutant Consortium, 2012).
172 The fourth strain harbors *fzr-1(ku298)*, a hypomorphic allele, as FZR-1 function is required for
173 viability (Fay et al., 2002). However, regardless of their genotype, live imaging and subsequent
174 quantification of CDK activity demonstrated that they all possessed a post-mitotic, invasive AC
175 (Fig. 2; Table 1).
176
177 These results were consistent with what we found after depleting CKI-1 by RNAi in a wild-type
178 background of the three-color imaging strain (Fig. S1B,C; Table 1). We next explored whether
179 we could induce AC proliferation by depleting CKI-1 in each mutant background. Following *cki-*
180 *1(RNAi)* treatment, we observed ≥2 ACs in 13%, 15%, 35%, and 81% of *cki-2(ok2105)*, *lin-*
181 *35(n745)*, *fzr-1(ku298)*, and *lin-23(e1883)* animals, respectively (Fig. 2). Compared to mutant
182 controls, this corresponded to a significant increase in AC-specific CDK activity (0.14 ± 0.03 (n =
183 30) vs. 0.55 ± 0.50 (n = 39), 0.15 ± 0.04 (n = 31) vs. 0.77 ± 0.52 (n = 54), 0.17 ± 0.05 (n = 32)
184 vs. 0.64 ± 0.57 (n = 55), and 0.13 ± 0.03 (n = 34) vs. 1.22 ± 0.72 (n = 111), respectively).
185 Additionally, we observed an increase in the percentage of proliferating ACs that underwent BM
186 invasion (Table 1). Overall, these findings, together with our *cki-1(RNAi)* results in RNAi-
187 sensitive backgrounds (Fig. 1D,E; Fig. S1A), highlight the critical role of CKI-1 in maintaining the
188 post-mitotic state of the AC.
189
190 **Maintenance of the post-mitotic state is not required for AC invasion**
191
192 To further investigate the lack of AC invasion defects following robust cell cycle induction (Table
193 1), we collected time-lapse movies of cycling ACs from pre-invasion to post-invasion using a
194 variant of the three-color imaging strain (Fig. 3; Fig. S3). Included in this strain is an AC-specific
195 F-actin probe, *cdh-3p*::mCherry::moesinABD, which we paired with a ubiquitous CDK activity
196 sensor, DHB::2xmTurquoise2, and an endogenous *lam-2* translational reporter, LAM-
197 2::mNeonGreen. We also added the *fzr-1(ku298)* hypomorphic allele rather than the *lin-*
198 *23(e1883)* null allele, as *fzr-1(ku298)* animals were easier to propagate and had the next
199 highest penetrance of the proliferative AC phenotype in the presence of *cki-1(RNAi)* (Fig. 2C,G;
200 Table 1).
201
202 Prior to time-lapse imaging, we captured static images of the invasive AC in *fzr-1(ku298);*
203 *control(RNAi)* animals (Fig. 3A), which allowed us to obtain a baseline level of CDK activity
204 values (0.31 ± 0.05 (n = 23)). This baseline allowed us to selectively record the activity of pre-

205 invasive ACs in *fzr-1(ku298); cki-1(RNAi)* animals that had already started cycling. Remarkably,
206 we collected five time-lapse datasets in which single or multiple cycling, pre-invasive ACs
207 showed an enrichment of the F-actin probe at the invasive membrane (Hagedorn et al., 2013)
208 (1.74 ± 0.36 (n = 7)), followed by successful invasion of the underlying BM (Fig. 3B; Movie 1). In
209 one of these datasets, we observed the division of a pre-invasive AC, with both daughter cells
210 re-entering the cell cycle before invading (Fig. S3). Altogether, these observations led us to
211 conclude that maintenance of the post-mitotic state is not required for AC invasion.
212
213 **The pro-invasive GRN is functionally intact in proliferating, invasive ACs**
214
215 After finding that direct disruption of the cell cycle leads to proliferating, invasive ACs, we
216 investigated whether these ACs maintain a functional pro-invasive gene regulatory network
217 (GRN) (Deng et al., 2020; Medwig-Kinney et al., 2020). This GRN consists of a cell cycle-
218 dependent and cell cycle-independent arm. We predicted that gene expression in both arms
219 would remain unchanged in proliferating, invasive ACs.
220
221 To test our hypothesis, we quantified endogenous levels of NHR-67, which is the distal
222 transcription factor in the cell cycle-dependent arm and is upstream of CKI-1. Additionally, we
223 quantified transcriptional levels of the matrix metalloproteinase (MMP) gene, *zmp-1*, which is
224 one of the downstream effectors of the cell cycle-independent arm. We quantified these levels in
225 two separate *fzr-1(ku298)* strains, each carrying most, if not all, of the original three-color
226 imaging alleles in the presence of *cki-1(RNAi)*. In one strain, we inserted an mNeonGreen tag
227 into the C-terminus of the endogenous *nhr-67* locus using CRISPR/Cas9 (Paix et al., 2015). In
228 the other strain, we exchanged the endogenous *lag-2* transcriptional reporter, LAG-
229 2::P2A::H2B::mTurquoise2, for a *zmp-1* transcriptional reporter transgene, *zmp-1p*::CFP (Inoue
230 et al., 2002). Supporting our prediction, NHR-67::mNeonGreen expression decreased by only
231 17% in proliferating, invasive ACs (Fig. 4A,B), whereas *zmp-1p*::CFP expression decreased by
232 73% in proliferating, invasive ACs (Fig. 4C,D). However, given that depletion of GRN
233 transcription factors results in proliferating, non-invasive ACs and a complete loss of *zmp-1*
234 transgene expression (Hwang et al., 2007; Matus et al., 2015; Medwig-Kinney et al., 2020;
235 Rimann and Hajnal, 2007; Sherwood et al., 2005), these data indicate that the pro-invasive
236 GRN is functionally intact in proliferating, invasive ACs (Fig. 4E).
237
238 **Conclusions**

239

240 In this study, we establish a critical role for CKI-1 in maintaining the post-mitotic state of the AC.
241 However, without knowing the null phenotype of *cki-1*, it remains difficult to ascertain the
242 redundancies, if any, in the AC cell cycle machinery (Matus et al., 2015). In *C. elegans*, there
243 are two CDK inhibitors: CKI-1 and CKI-2. Recent work has shown that *cki-2* becomes
244 upregulated in terminally differentiated vulval cells that are devoid of *cki-1* expression (Portegijs,
245 2019). This same compensatory relationship may exist in the AC. This could in part explain the
246 enhanced penetrance of the proliferative AC phenotype following loss of CKI-1 in *rrf-3(pk1426)*
247 and *cki-2(ok2105)* null mutant backgrounds (Fig. 1D,E; Fig. 2A,E). Interestingly, we observed a
248 synergistic increase in the number of proliferating ACs in *lin-23(e1883); cki-1(RNAi)* animals
249 (Fig. 2D,H). Perhaps complete loss of CKI-1, CKI-2, and LIN-23 is required to achieve a fully
250 penetrant ≥2 AC phenotype. We also do not know the null phenotype of *fzr-1*. Therefore, it may
251 have a more significant role in maintaining the post-mitotic state of the AC. However, use of the
252 *fzr-1(ku298)* hypomorphic allele sufficiently triggered cell cycle entry in post-mitotic neurons
253 (The et al., 2015). Lastly, as LIN-35 functions in both canonical cell cycle regulation and
254 negative regulation of RNAi pathways (Boxem and van den Heuvel, 2001; Boxem and van den
255 Heuvel, 2002; Lehner et al., 2006; Wang et al., 2005), we cannot rule out the possibility that the
256 *lin-35(n745)* null allele is simply enhancing the efficiency of *cki-1(RNAi)* (Fig. 2B,F). These
257 ambiguities could be addressed in future studies by creating and/or combining conditional null
258 alleles using the auxin-inducible degron (AID) system (Ashley et al., 2021; Hills-Muckey et al.,
259 2021; Martinez et al., 2020; Negishi et al., 2021; Sepers et al., 2022; Xiao et al., 2023; Zhang et
260 al., 2015) or an analogous approach (Nance and Frøkjær-Jensen, 2019).
261

262 Finally, we demonstrate that AC invasion can occur irrespective of cell cycle state (Fig. 3),
263 which breaks the dichotomy between invasion and proliferation in *C. elegans* (Matus et al.,
264 2015). We evaluated the functionality of the GRN that controls AC invasion (Deng et al., 2020;
265 Medwig-Kinney et al., 2020), specifically examining the expression of two components: NHR-67
266 and *zmp-1* (Fig. 4). These components provide readouts of the cell cycle-dependent and cell
267 cycle-independent arm, respectively. We observed a considerable reduction in *zmp-1*
268 expression in proliferating, invasive ACs, but not in NHR-67 expression. The presence of
269 reduced *zmp-1* expression in these cells suggests that cell cycle progression downregulates the
270 production of MMPs independently of the GRN components that transcriptionally regulate them
271 (Medwig-Kinney et al., 2020). However, MMPs are not necessary for AC invasion (Kelley et al.,
272 2019). In the absence of MMPs, the AC adapts by expanding its invasive F-actin network and

physically forcing its way through the underlying BM in an ATP-dependent manner. Given that cell invasion and proliferation are both energy-intensive processes, future investigation is warranted into whether they can occur simultaneously in the absence of MMPs. To our knowledge, this is the first example in development where an invasively differentiated cell can perform its specialized function while proliferating. Although evidence suggests that tumor cells must alternate between proliferative and invasive states (Kohrman and Matus, 2017; Mondal et al., 2022), additional research targeting the cell cycle in invasive tumor cells is required to determine the necessity of this phenotypic switch.

MATERIALS AND METHODS

Strains

All strains were grown and maintained following standard procedures (Brenner, 1974). A complete list of strains used in this study is available in Table S1.

Alleles

The following alleles were used in this study: *qyIs102[fos-1ap::rde-1]* (Hagedorn et al., 2009); **LG I** *bmd156[rps-27p::DHB::2xmKate2]* (Adikes et al., 2020), *bmd294[rps-27p::DHB::2xmTurquoise2]* (this study), and *lin-35(n745)* (Lu and Horvitz, 1998); **LG II** *bmd168[rps-27p::DHB::2xmKate2]* (Adikes et al., 2020), *lin-23(e1883)* (Kipreos et al., 2000), *cki-1(gk132)* (The *C. elegans* Deletion Mutant Consortium, 2012), *cdc-14(he141)* (Saito et al., 2004), *fzr-1(ku298)* (Fay et al., 2002), *cki-2(ok2105)* (The *C. elegans* Deletion Mutant Consortium, 2012), and *rrf-3(pk1426)* (Simmer et al., 2002); **LG IV** *qyIs10[lam-1p::lam-1::GFP]* (Ziel et al., 2009), *qyIs225[cdh-3p::mCherry::moesinABD]* (Matus et al., 2015), and *nhr-67(wy1787[nhr-67::mNeonGreen])* (this study); **LG V** *lag-2(bmd202[lag-2::P2A::H2B::mTurquoise2])* (Medwig-Kinney et al., 2022), *rde-1(ne219)* (Tabara et al., 1999), and *syIs67[zmp-1p::CFP]* (Inoue et al., 2002); **LG X** *lam-2(qy20[lam-2::mNeonGreen])* (Jayadev et al., 2019) and *qyIs24[cdh-3p::mCherry::PLCδPH]* (Ziel et al., 2009).

Generation of the transgenic bmd294 allele

306 Both pWZ186 (Addgene plasmid #163641) and a plasmid containing 2xmTurquoise2 were
307 double digested with Bsu36I and NgoMIV to excise 2xmKate2 and 2xmTurquoise2,
308 respectively. pMAM038 (rps-27p::DHB::2xmTurquoise2) was cloned by T4 ligation using the
309 backbone from pWZ186 and 2xmTurquoise2 as an insert. After sequence confirmation,
310 pMAM038 was used as a repair template for insertion into the genome at a safe harbor site on
311 chromosome I corresponding to the MosSCI insertion site, ttTi4348 (Frøkjær-Jensen et al.,
312 2012). pAP082 was used as the sgRNA plasmid for chromosome I insertion by CRISPR/Cas9
313 (Pani and Goldstein, 2018). Young adults were transformed using standard microinjection
314 techniques, and integrants were identified through the SEC method (Dickinson et al., 2015).
315
316 *Generation of the endogenous wy1787 allele*
317
318 A repair template containing 30xlinker-mNeonGreen, with homology at the 5' and 3' ends to the
319 C-terminus of the *nhr-67* locus, was PCR amplified from pJW2171 (Addgene plasmid #163095)
320 and concentrated using a PCR purification kit (Qiagen). 3 µl of 10 µM stock tracRNA (IDT) was
321 incubated with 0.5 µl of a 100 µM crRNA (IDT) for 5 min at 95°C followed by 5 min at 25°C.
322 Immediately following incubation, the tracRNA:cRNA mixture was incubated with 0.5 µl of Alt-R
323 Cas9 protein (IDT) for 10 min at 37°C. The repair template and co-injection marker (pRF6) were
324 combined with the mixture to a final concentration of 200 ng/µl and 50 ng/µl, respectively, for a
325 final injection mix volume of 10 µl. Adult worms possessing no more than a single row of eggs
326 were transformed using standard microinjection techniques. Roller F1 progeny were singled out,
327 and F2 progeny were genotyped for insertions (Paix et al., 2015). The sequence of the PCR
328 primers and guide are available in Tables S2 and S3, respectively.
329
330 *RNAi*
331
332 All RNAi experiments were performed by first synchronizing animals at the L1 larval stage using
333 the bleaching technique (Porta-de-la-Riva et al., 2012). These animals were then fed bacteria
334 expressing the T444T-based RNAi construct for *cki-1* until the mid-L3 larval stage (P6.p four-cell
335 stage), when AC invasion normally occurs (Sherwood and Sternberg, 2003). Control animals
336 were fed bacteria carrying the empty T444T vector.
337
338 *Generation of a T444T-based RNAi construct for cki-1*
339

340 A T444T-based RNAi construct targeting *cki-1* was generated by inserting a 552 bp synthetic
341 DNA fragment, based on the *cki-1* cDNA sequence from WormBase (Davis et al., 2022), into
342 the T444T vector (Addgene plasmid #113081) using the BglII and XhoI restriction sites (Sturm
343 et al., 2018). The synthetic DNA was purchased from IDT as a gBlock with homology arms to
344 T444T for Gibson assembly. The sequence of the synthetic DNA is available in Table S4.
345
346 *Image acquisition*
347
348 Images were acquired using a spinning disk confocal microscope supported by Nobska
349 Imaging. This confocal system consists of a Hamamatsu ORCA EM-CCD camera mounted on
350 an upright Zeiss Axio Imager.A2, equipped with a Borealis-modified Yokogawa CSU-10
351 spinning disk scanning unit with 6 solid state (405, 440, 488, 514, 561, and 640 nm) lasers and
352 a Zeiss Plan-Apochromat 100x/1.4 oil DIC objective.
353
354 For static imaging, animals were anesthetized by placing them into a drop of M9 on a 5%
355 agarose pad containing 7 mM sodium azide and securing them with a coverslip. Time-lapse
356 imaging was performed using a modified version of a previously published protocol (Kelley et
357 al., 2017), as described in Adikes et al. (2020).
358
359 *Imaging processing and analysis*
360
361 The acquired images were processed using ImageJ/Fiji (Schneider et al., 2012). DHB ratios
362 were quantified as previously described (Adikes et al., 2020). NHR-67::mNeonGreen and *zmp-*
363 *1*::CFP fluorescence were quantified as previously described (Medwig-Kinney et al., 2020). AC
364 invasion was defined as the complete loss of fluorescent BM signal underneath the AC. Plots
365 were generated using Prism software, and figures, including cartoons, were created using a
366 combination of Adobe Photoshop and Illustrator.
367
368 *Statistics*
369
370 A power analysis was performed to determine the number of animals (N) needed per
371 experiment (Pollard et al., 2019). The figure legends specify the measures of central tendency,
372 error bars, numeric *P*-values, and statistical tests used.
373

Acknowledgements

We thank Nicholas Palmisano, Sam Stettnisch, and Abigail Nishimura for their comments and suggestions.

Data availability

All relevant data can be found within the article and its supplementary information.

Competing interests

D.Q.M. is a paid employee of Arcadia Science.

Author contributions

Conceptualization: M.A.Q.M., D.Q.M.; Methodology: M.A.Q.M., D.Q.M.; Validation: M.A.Q.M., C.Z.Z.; Formal analysis: M.A.Q.M.; Investigation: M.A.Q.M., C.Z.Z., F.E.Q.M.; Resources: F.E.Q.M., C.Y., W.Z.; Writing – original draft: M.A.Q.M.; Writing – review and editing: M.A.Q.M., D.Q.M.; Visualization: M.A.Q.M., C.Z.Z., D.Q.M.; Supervision: B.L.M., D.Q.M.; Project administration: M.A.Q.M.; Funding acquisition: K.S., B.L.M., D.Q.M.

Funding

M.A.Q.M. is supported by the National Cancer Institute (F30CA257383), F.E.Q.M. is supported by the National Institute of General Medical Sciences Diversity Supplement Program (R01GM121597), C.Y. is supported by the Human Frontiers Science Program (LT000127/2016-L), and K.S. is a Howard Hughes Medical Institute Investigator. Additionally, both B.L.M. and D.Q.M. are supported by the Damon Runyon Cancer Research Foundation (DRR4714), and D.Q.M. is also supported by the National Institute of General Medical Sciences (R01GM121597).

408 **REFERENCES**

409

410 Adikes, R. C., Kohrman, A. Q., Martinez, M. A. Q., Palmisano, N. J., Smith, J. J., Medwig-
411 Kinney, T. N., Min, M., Sallee, M. D., Ahmed, O. B., Kim, N., et al. (2020). Visualizing the
412 metazoan proliferation-quiescence decision in vivo. *eLife* 9, e63265.

413 Ajioka, I., Martins, R. A. P., Bayazitov, I. T., Donovan, S., Johnson, D. A., Frase, S., Cicero, S.
414 A., Boyd, K., Zakharenko, S. S. and Dyer, M. A. (2007). Differentiated Horizontal
415 Interneurons Clonally Expand to Form Metastatic Retinoblastoma in Mice. *Cell* 131,
416 378–390.

417 Ashley, G. E., Duong, T., Levenson, M. T., Martinez, M. A. Q., Johnson, L. C., Hibshman, J. D.,
418 Saeger, H. N., Palmisano, N. J., Doonan, R., Martinez-Mendez, R., et al. (2021). An
419 expanded auxin-inducible degron toolkit for *Caenorhabditis elegans*. *Genetics* 217,
420 iyab006.

421 Boxem, M. and van den Heuvel, S. (2001). *lin-35* Rb and *cki-1* Cip/Kip cooperate in
422 developmental regulation of G1 progression in *C. elegans*. *Development* 128, 4349–
423 4359.

424 Boxem, M. and van den Heuvel, S. (2002). *C. elegans* Class B Synthetic Multivulva Genes Act
425 in G1 Regulation. *Current Biology* 12, 906–911.

426 Brenner, S. (1974). The genetics of *Caenorhabditis elegans*. *Genetics* 77, 71–94.

427 Buck, S. H., Chiu, D. and Saito, R. M. (2009). The cyclin-dependent kinase inhibitors, *cki-1* and
428 *cki-2*, act in overlapping but distinct pathways to control cell-cycle quiescence during *C.*
429 *elegans* development. *Cell Cycle* 8, 2613–2620.

430 Buttitta, L. A. and Edgar, B. A. (2007). Mechanisms controlling cell cycle exit upon terminal
431 differentiation. *Current Opinion in Cell Biology* 19, 697–704.

432 Clayton, J. E., van den Heuvel, S. J. L. and Saito, R. M. (2008). Transcriptional control of cell-
433 cycle quiescence during *C. elegans* development. *Developmental Biology* 313, 603–613.

434 Davis, P., Zarowiecki, M., Arnaboldi, V., Becerra, A., Cain, S., Chan, J., Chen, W. J., Cho, J., da
435 Veiga Beltrame, E., Diamantakis, S., et al. (2022). WormBase in 2022—data, processes,
436 and tools for analyzing *Caenorhabditis elegans*. *Genetics* 220, iyac003.

437 Deng, T., Stempor, P., Appert, A., Daube, M., Ahringer, J., Hajnal, A. and Lattmann, E. (2020).
438 The *Caenorhabditis elegans* homolog of the Evi1 proto-oncogene, *egl-43*, coordinates
439 G1 cell cycle arrest with pro-invasive gene expression during anchor cell invasion. *PLoS*
440 *Genet* 16, e1008470.

441 Dickinson, D. J., Pani, A. M., Heppert, J. K., Higgins, C. D. and Goldstein, B. (2015).
442 Streamlined Genome Engineering with a Self-Excising Drug Selection Cassette.
443 *Genetics* 200, 1035–1049.

444 Fay, D. S., Keenan, S. and Han, M. (2002). *fzr-1* and *lin-35* /Rb function redundantly to control
445 cell proliferation in *C. elegans* as revealed by a nonbiased synthetic screen. *Genes Dev.*
446 16, 503–517.

447 Feng, H., Zhong, W., Punkosdy, G., Gu, S., Zhou, L., Seabolt, E. K. and Kipreos, E. T. (1999).
448 CUL-2 is required for the G1-to-S-phase transition and mitotic chromosome
449 condensation in *Caenorhabditis elegans*. *Nature Cell Biology* 1, 486–492.

450 Frøkjær-Jensen, C., Davis, M. W., Ailion, M. and Jorgensen, E. M. (2012). Improved Mos1-
451 mediated transgenesis in *C. elegans*. *Nat Methods* 9, 117–118.

452 Fukuyama, M., Gendreau, S. B., Derry, W. B. and Rothman, J. H. (2003). Essential embryonic
453 roles of the CKI-1 cyclin-dependent kinase inhibitor in cell-cycle exit and morphogenesis
454 in *C. elegans*. *Developmental Biology* 260, 273–286.

455 Haass, N. K., Beaumont, K. A., Hill, D. S., Anfosso, A., Mrass, P., Munoz, M. A., Kinjyo, I. and
456 Weninger, W. (2014). Real-time cell cycle imaging during melanoma growth, invasion,
457 and drug response. *Pigment Cell & Melanoma Research* 27, 764–776.

458 Hagedorn, E. J., Yashiro, H., Ziel, J. W., Ihara, S., Wang, Z. and Sherwood, D. R. (2009).
459 Integrin Acts Upstream of Netrin Signaling to Regulate Formation of the Anchor Cell's
460 Invasive Membrane in *C. elegans*. *Developmental Cell* 17, 187–198.

461 Hagedorn, E. J., Ziel, J. W., Morrissey, M. A., Linden, L. M., Wang, Z., Chi, Q., Johnson, S. A.
462 and Sherwood, D. R. (2013). The netrin receptor DCC focuses invadopodia-driven
463 basement membrane transmigration in vivo. *Journal of Cell Biology* 201, 903–913.

464 Hills-Muckey, K., Martinez, M. A. Q., Stec, N., Hebbar, S., Saldanha, J., Medwig-Kinney, T. N.,
465 Moore, F. E. Q., Ivanova, M., Morao, A., Ward, J. D., et al. (2021). An engineered,
466 orthogonal auxin analog/AtTIR1(F79G) pairing improves both specificity and efficacy of
467 the auxin degradation system in *Caenorhabditis elegans*. *Genetics* 220, iyab174.

468 Hong, Y., Roy, R. and Ambros, V. (1998). Developmental regulation of a cyclin-dependent
469 kinase inhibitor controls postembryonic cell cycle progression in *Caenorhabditis elegans*.
470 *Development* 125, 3585–3597.

471 Hwang, B. J., Meruelo, A. D. and Sternberg, P. W. (2007). *C. elegans* EVI1 proto-oncogene,
472 EGL-43, is necessary for Notch-mediated cell fate specification and regulates cell
473 invasion. *Development* 134, 669–679.

474 Inoue, T., Sherwood, D. R., Aspöck, G., Butler, J. A., Gupta, B. P., Kirouac, M., Wang, M., Lee,
475 P.-Y., Kramer, J. M., Hope, I., et al. (2002). Gene expression markers for *Caenorhabditis*
476 *elegans* vulval cells. *Mechanisms of Development* 119, S203–S209.

477 Jayadev, R., Chi, Q., Keeley, D. P., Hastie, E. L., Kelley, L. C. and Sherwood, D. R. (2019). α-
478 Integrins dictate distinct modes of type IV collagen recruitment to basement membranes.
479 *Journal of Cell Biology* 218, 3098–3116.

480 Kelley, L. C., Wang, Z., Hagedorn, E. J., Wang, L., Shen, W., Lei, S., Johnson, S. A. and
481 Sherwood, D. R. (2017). Live-cell confocal microscopy and quantitative 4D image
482 analysis of anchor-cell invasion through the basement membrane in *Caenorhabditis*
483 *elegans*. *Nature Protocols* 12, 2081–2096.

484 Kelley, L. C., Chi, Q., Cáceres, R., Hastie, E., Schindler, A. J., Jiang, Y., Matus, D. Q., Plastino,
485 J. and Sherwood, D. R. (2019). Adaptive F-Actin Polymerization and Localized ATP
486 Production Drive Basement Membrane Invasion in the Absence of MMPs.
487 *Developmental Cell* 48, 313-328.e8.

488 Kipreos, E. T. and van den Heuvel, S. (2019). Developmental Control of the Cell Cycle: Insights
489 from *Caenorhabditis elegans*. *Genetics* 211, 797–829.

490 Kipreos, E. T., Lander, L. E., Wing, J. P., He, W. W. and Hedgecock, E. M. (1996). *cul-1* Is
491 Required for Cell Cycle Exit in C. elegans and Identifies a Novel Gene Family. *Cell* 85,
492 829–839.

493 Kipreos, E. T., Gohel, S. P. and Hedgecock, E. M. (2000). The *C. elegans* F-box/WD-repeat
494 protein LIN-23 functions to limit cell division during development. *Development* 127,
495 5071–5082.

496 Kohrman, A. Q. and Matus, D. Q. (2017). Divide or Conquer: Cell Cycle Regulation of Invasive
497 Behavior. *Trends in Cell Biology* 27, 12–25.

498 Lehner, B., Calixto, A., Crombie, C., Tischler, J., Fortunato, A., Chalfie, M. and Fraser, A. G.
499 (2006). Loss of LIN-35, the *Caenorhabditis elegans* ortholog of the tumor suppressor
500 p105Rb, results in enhanced RNA interference. *Genome Biology* 7, R4.

501 Lu, X. and Horvitz, H. R. (1998). *lin-35* and *lin-53*, Two Genes that Antagonize a *C. elegans* Ras
502 Pathway, Encode Proteins Similar to Rb and Its Binding Protein RbAp48. *Cell* 95, 981–
503 991.

504 Martinez, M. A. Q. and Matus, D. Q. (2022). CDK activity sensors: genetically encoded
505 ratiometric biosensors for live analysis of the cell cycle. *Biochemical Society*
506 *Transactions* 50, 1081–1090.

507 Martinez, M. A. Q., Kinney, B. A., Medwig-Kinney, T. N., Ashley, G., Ragle, J. M., Johnson, L.,
508 Aguilera, J., Hammell, C. M., Ward, J. D. and Matus, D. Q. (2020). Rapid Degradation of
509 *Caenorhabditis elegans* Proteins at Single-Cell Resolution with a Synthetic Auxin. *G3*
510 *Genes|Genomes|Genetics* 10, 267–280.

511 Matus, D. Q., Li, X.-Y., Durbin, S., Agarwal, D., Chi, Q., Weiss, S. J. and Sherwood, D. R.
512 (2010). In Vivo Identification of Regulators of Cell Invasion Across Basement
513 Membranes. *Sci. Signal.* 3, ra35.

514 Matus, D. Q., Lohmer, L. L., Kelley, L. C., Schindler, A. J., Kohrman, A. Q., Barkoulas, M.,
515 Zhang, W., Chi, Q. and Sherwood, D. R. (2015). Invasive Cell Fate Requires G1 Cell-
516 Cycle Arrest and Histone Deacetylase-Mediated Changes in Gene Expression.
517 *Developmental Cell* 35, 162–174.

518 Medwig-Kinney, T. N., Smith, J. J., Palmisano, N. J., Tank, S., Zhang, W. and Matus, D. Q.
519 (2020). A developmental gene regulatory network for *C. elegans* anchor cell invasion.
520 *Development* 147, dev.185850.

521 Medwig-Kinney, T. N., Sirota, S. S., Gibney, T. V., Pani, A. M. and Matus, D. Q. (2022). An *in*
522 *vivo* toolkit to visualize endogenous LAG-2/Delta and LIN-12/Notch signaling in *C.*
523 *elegans*. *MicroPublication Biology* 2022, 10.17912/micropub.biology.000602.

524 Mondal, C., Gacha-Garay, M. J., Larkin, K. A., Adikes, R. C., Di Martino, J. S., Chien, C.-C.,
525 Fraser, M., Eni-aganga, I., Agullo-Pascual, E., Cialowicz, K., et al. (2022). A proliferative
526 to invasive switch is mediated by srGAP1 downregulation through the activation of TGF-
527 β2 signaling. *Cell Reports* 40,.

528 Nance, J. and Frøkjær-Jensen, C. (2019). The *Caenorhabditis elegans* Transgenic Toolbox.
529 *Genetics* 212, 959–990.

530 Nayak, S., Santiago, F. E., Jin, H., Lin, D., Schedl, T. and Kipreos, E. T. (2002). The
531 *Caenorhabditis elegans* Skp1-Related Gene Family: Diverse Functions in Cell
532 Proliferation, Morphogenesis, and Meiosis. *Current Biology* 12, 277–287.

533 Negishi, T., Kitagawa, S., Horii, N., Tanaka, Y., Haruta, N., Sugimoto, A., Sawa, H., Hayashi, K.,
534 Harata, M. and Kanemaki, M. T. (2021). The auxin-inducible degron 2 (AID2) system
535 enables controlled protein knockdown during embryogenesis and development in
536 *Caenorhabditis elegans*. *Genetics* 220, iyab218.

537 Paix, A., Folkmann, A., Rasoloson, D. and Seydoux, G. (2015). High Efficiency, Homology-
538 Directed Genome Editing in *Caenorhabditis elegans* Using CRISPR-Cas9
539 Ribonucleoprotein Complexes. *Genetics* 201, 47–54.

540 Pani, A. M. and Goldstein, B. (2018). Direct visualization of a native Wnt in vivo reveals that a
541 long-range Wnt gradient forms by extracellular dispersal. *eLife* 7, e38325.

542 Pollard, D. A., Pollard, T. D. and Pollard, K. S. (2019). Empowering statistical methods for
543 cellular and molecular biologists. *MBoC* 30, 1359–1368.

544 Porta-de-la-Riva, M., Fontrodona, L., Villanueva, A. and Cerón, J. (2012). Basic *Caenorhabditis*
545 *elegans* Methods: Synchronization and Observation. *JoVE* e4019.

546 Portegijs, V. (2019). Developmental control of the *C. elegans* cell cycle.

547 Rimann, I. and Hajnal, A. (2007). Regulation of anchor cell invasion and uterine cell fates by the
548 *egl-43* Evi-1 proto-oncogene in *Caenorhabditis elegans*. *Developmental Biology* 308,
549 187–195.

550 Roy, S. H., Clayton, J. E., Holmen, J., Beltz, E. and Saito, R. M. (2011). Control of Cdc14
551 activity coordinates cell cycle and development in *Caenorhabditis elegans*. *Mechanisms*
552 *of Development* 128, 317–326.

553 Roy, S. H., Tobin, D. V., Memar, N., Beltz, E., Holmen, J., Clayton, J. E., Chiu, D. J., Young, L.
554 D., Green, T. H., Lubin, I., et al. (2014). A Complex Regulatory Network Coordinating
555 Cell Cycles During *C. elegans* Development Is Revealed by a Genome-Wide RNAi
556 Screen. *G3 Genes*|*Genomes*|*Genetics* 4, 795–804.

557 Ruijtenberg, S. and van den Heuvel, S. (2016). Coordinating cell proliferation and differentiation:
558 Antagonism between cell cycle regulators and cell type-specific gene expression. *Cell*
559 *Cycle* 15, 196–212.

560 Sage, C., Huang, M., Karimi, K., Gutierrez, G., Vollrath, M. A., Zhang, D.-S., García-Añoveros,
561 J., Hinds, P. W., Corwin, J. T., Corey, D. P., et al. (2005). Proliferation of Functional Hair
562 Cells in Vivo in the Absence of the Retinoblastoma Protein. *Science* 307, 1114–1118.

563 Saito, R. M., Perreault, A., Peach, B., Satterlee, J. S. and van den Heuvel, S. (2004). The CDC-
564 14 phosphatase controls developmental cell-cycle arrest in *C. elegans*. *Nat Cell Biol* 6,
565 777–783.

566 Schneider, C. A., Rasband, W. S. and Eliceiri, K. W. (2012). NIH Image to ImageJ: 25 years of
567 image analysis. *Nat Methods* 9, 671–675.

568 Sepers, J. J., Verstappen, N. H. M., Vo, A. A., Ragle, J. M., Ruijtenberg, S., Ward, J. D. and
569 Boxem, M. (2022). The mIAA7 degron improves auxin-mediated degradation in *C.*
570 *elegans*. *G3 Genes*|*Genomes*|*Genetics* 12, jkac222.

571 Sherwood, D. R. and Sternberg, P. W. (2003). Anchor Cell Invasion into the Vulval Epithelium in
572 *C. elegans*. *Developmental Cell* 5, 21–31.

573 Sherwood, D. R., Butler, J. A., Kramer, J. M. and Sternberg, P. W. (2005). FOS-1 Promotes
574 Basement-Membrane Removal during Anchor-Cell Invasion in *C. elegans*. *Cell* 121,
575 951–962.

576 Simmer, F., Tijsterman, M., Parrish, S., Koushika, S. P., Nonet, M. L., Fire, A., Ahringer, J. and
577 Plasterk, R. H. A. (2002). Loss of the Putative RNA-Directed RNA Polymerase RRF-3
578 Makes *C. elegans* Hypersensitive to RNAi. *Current Biology* 12, 1317–1319.

579 Smith, J. J., Xiao, Y., Parsan, N., Medwig-Kinney, T. N., Martinez, M. A. Q., Moore, F. E. Q.,
580 Palmisano, N. J., Kohrman, A. Q., Chandhok Delos Reyes, M., Adikes, R. C., et al.
581 (2022). The SWI/SNF chromatin remodeling assemblies BAF and PBAF differentially
582 regulate cell cycle exit and cellular invasion *in vivo*. *PLoS Genet* 18, e1009981.

583 Soufi, A. and Dalton, S. (2016). Cycling through developmental decisions: how cell cycle
584 dynamics control pluripotency, differentiation and reprogramming. *Development* 143,
585 4301–4311.

586 Spencer, S. L., Cappell, S. D., Tsai, F.-C., Overton, K. W., Wang, C. L. and Meyer, T. (2013).
587 The Proliferation-Quiescence Decision Is Controlled by a Bifurcation in CDK2 Activity at
588 Mitotic Exit. *Cell* 155, 369–383.

589 Sturm, Á., Saskői, É., Tibor, K., Weinhardt, N. and Vellai, T. (2018). Highly efficient RNAi and
590 Cas9-based auto-cloning systems for *C. elegans* research. *Nucleic Acids Research* 46,
591 e105.

592 Tabara, H., Sarkissian, M., Kelly, W. G., Fleenor, J., Grishok, A., Timmons, L., Fire, A. and
593 Mello, C. C. (1999). The *rde-1* Gene, RNA Interference, and Transposon Silencing in *C.*
594 *elegans*. *Cell* 99, 123–132.

595 The, I., Ruijtenberg, S., Bouchet, B. P., Cristobal, A., Prinsen, M. B. W., van Mourik, T., Koreth,
596 J., Xu, H., Heck, A. J. R., Akhmanova, A., et al. (2015). Rb and FZR1/Cdh1 determine
597 CDK4/6-cyclin D requirement in *C. elegans* and human cancer cells. *Nature*
598 *Communications* 6, 5906.

599 The *C. elegans* Deletion Mutant Consortium (2012). Large-Scale Screening for Targeted
600 Knockouts in the *Caenorhabditis elegans* Genome. *G3 Genes|Genomes|Genetics* 2,
601 1415–1425.

602 Timmons, L. and Fire, A. (1998). Specific interference by ingested dsRNA. *Nature* 395, 854–
603 854.

604 van Rijnberk, L. M., van der Horst, S. E. M., van den Heuvel, S. and Ruijtenberg, S. (2017). A
605 dual transcriptional reporter and CDK-activity sensor marks cell cycle entry and
606 progression in *C. elegans*. *PLoS ONE* 12, e0171600.

607 Vittadello, S. T., McCue, S. W., Gunasingh, G., Haass, N. K. and Simpson, M. J. (2020).
608 Examining Go-or-Grow Using Fluorescent Cell-Cycle Indicators and Cell-Cycle-Inhibiting
609 Drugs. *Biophysical Journal* 118, 1243–1247.

610 Wang, D., Kennedy, S., Conte, D., Kim, J. K., Gabel, H. W., Kamath, R. S., Mello, C. C. and
611 Ruvkun, G. (2005). Somatic misexpression of germline P granules and enhanced RNA
612 interference in retinoblastoma pathway mutants. *Nature* 436, 593–597.

613 Xiao, Y., Yee, C., Zhao, C. Z., Martinez, M. A. Q., Zhang, W., Shen, K., Matus, D. Q. and
614 Hammell, C. (2023). An expandable FLP-ON::TIR1 system for precise spatiotemporal
615 protein degradation in *Caenorhabditis elegans*. *Genetics* iyad013.

616 Zhang, L., Ward, J. D., Cheng, Z. and Dernburg, A. F. (2015). The auxin-inducible degradation
617 (AID) system enables versatile conditional protein depletion in *C. elegans*. *Development*
618 142, 4374–4384.

619 Ziel, J. W., Hagedorn, E. J., Audhya, A. and Sherwood, D. R. (2009). UNC-6 (netrin) orients the
620 invasive membrane of the anchor cell in *C. elegans*. *Nat Cell Biol* 11, 183–189.

621
622
623
624
625
626
627
628
629
630
631

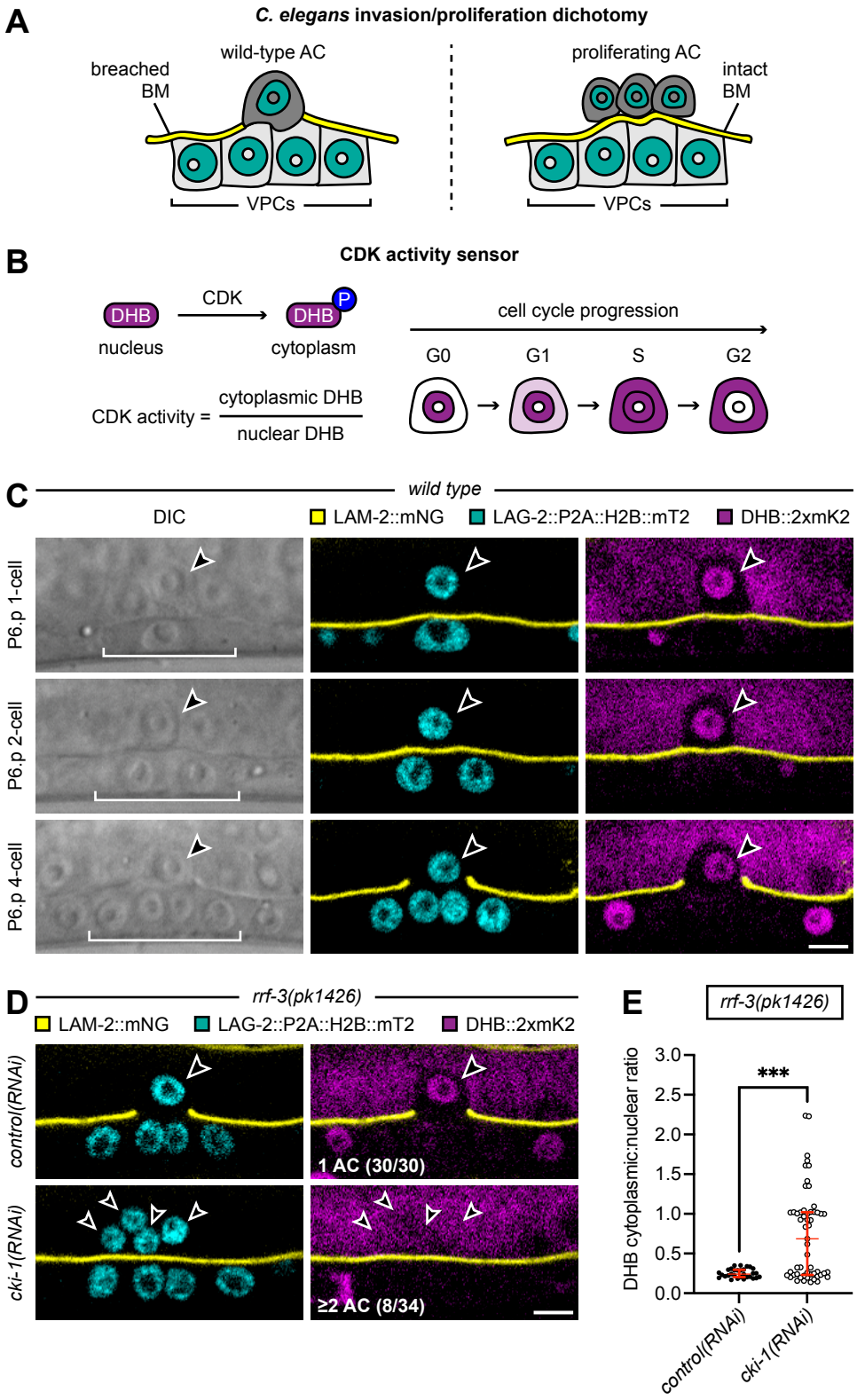
A
C. elegans invasion/proliferation dichotomy
wild-type AC
breached BM
VPCs
proliferating AC
intact BM
VPCs
B
CDK activity sensor
DHB
CDK
DHB
P
nucleus
cytoplasm
CDK activity = cytoplasmic DHB / nuclear DHB
cell cycle progression
G0
G1
S
G2
C
wild type
DIC
LAM-2::mNG
LAG-2::P2A::H2B::mT2
DHB::2xmK2
P6.p 1-cell
P6.p 2-cell
P6.p 4-cell
D
rrf-3(pk1426)
LAM-2::mNG
LAG-2::P2A::H2B::mT2
DHB::2xmK2
control(RNAi)
cki-1(RNAi)
1 AC (30/30)
≥2 AC (8/34)
E
rrf-3(pk1426)
DHB cytoplasmic:nuclear ratio
3.0
2.5
2.0
1.5
1.0
0.5
0.0
***
control(RNAi)
cki-1(RNAi)

632 **Figure 1. A moderate increase in AC proliferation is observed upon systemic depletion of**
633 **CKI-1.** (A) Schematic of the *C. elegans* invasion/proliferation dichotomy. (B) Schematic of the
634 CDK activity sensor, DHB, which is phosphorylated by CDK and translocates from the nucleus
635 to the cytoplasm in response to CDK activity during cell cycle progression. The equation used to
636 quantify CDK activity is shown. (C) DIC (left) and confocal images merging LAM-
637 2::mNeonGreen with LAG-2::P2A::H2B::mTurquoise2 (middle) and DHB::2xmKate2 (right) from
638 the P6.p 1-cell stage to the P6.p 4-cell stage are shown. Arrowheads and brackets indicate the
639 position of the AC and P6.p cells, respectively. The scale bar represents 5 μm. (D) Confocal
640 images merging LAM-2::mNeonGreen with LAG-2::P2A::H2B::mTurquoise2 (left) and
641 DHB::2xmKate2 (right) from the P6.p 4-cell stage are shown. Arrowheads indicate the position
642 of the AC(s) in *rrf-3(pk1426)* animals following *control(RNAi)* and *cki-1(RNAi)* treatment. The
643 scale bar represents 5 μm. (E) Plot displays median and IQR of DHB::2xmKate2 ratios in the
644 AC(s) of *rrf-3(pk1426)* animals following *control(RNAi)* and *cki-1(RNAi)* treatment ($N \geq 30$
645 animals per treatment). Statistical significance was determined by a Mann-Whitney test ($P <$
646 0.0004). See also Figure S1, S2.
647
648
649
650
651
652
653
654
655
656
657
658
659
660
661
662
663
664
665

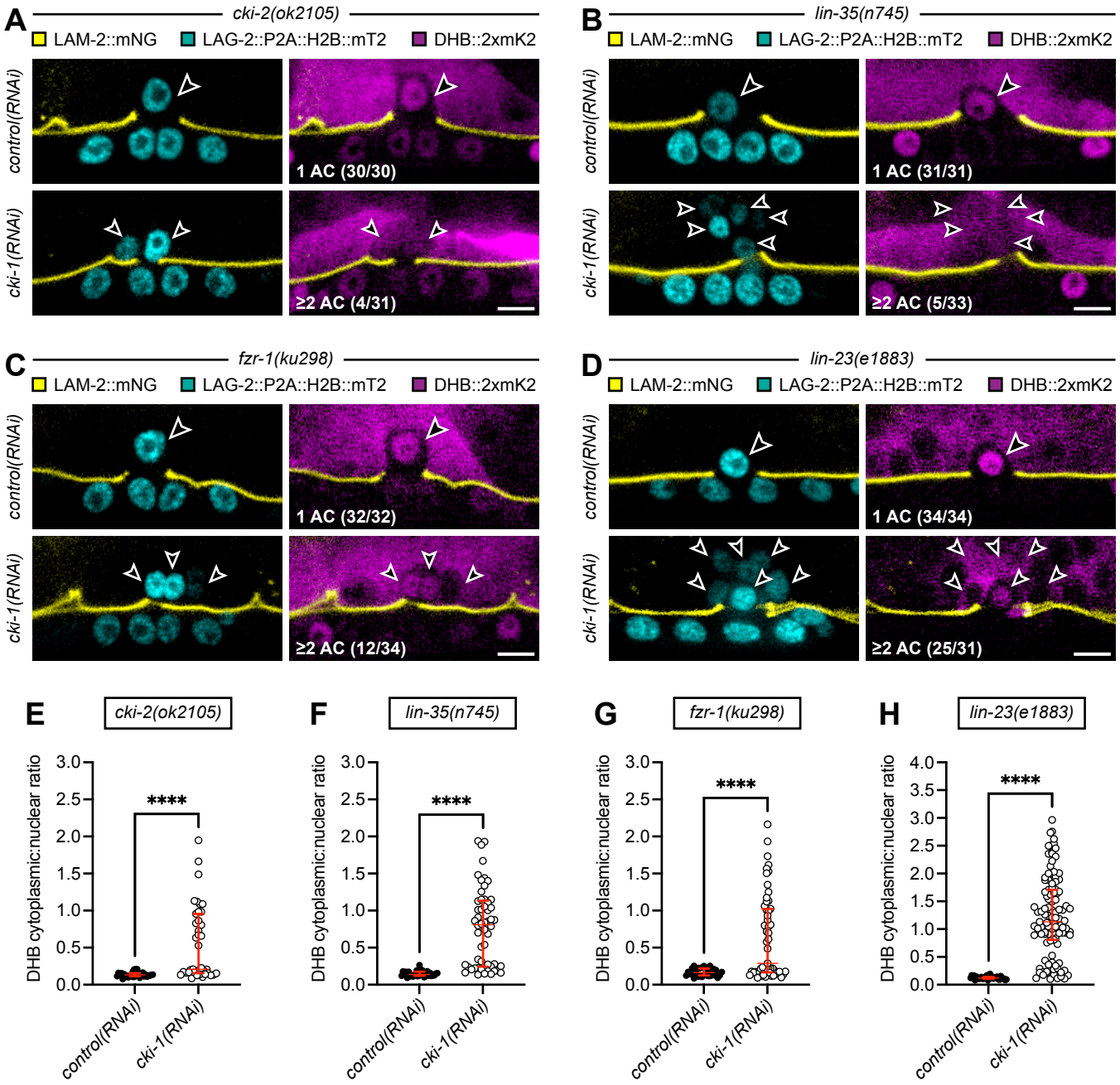
A
cki-2(ok2105)
LAM-2::mNG
LAG-2::P2A::H2B::mT2
DHB::2xmK2
control(RNAi)
cki-1(RNAi)
1 AC (30/30)
≥2 AC (4/31)
B
lin-35(n745)
1 AC (31/31)
≥2 AC (5/33)
C
fzr-1(ku298)
1 AC (32/32)
≥2 AC (12/34)
D
lin-23(e1883)
1 AC (34/34)
≥2 AC (25/31)
E
cki-2(ok2105)
F
lin-35(n745)
G
fzr-1(ku298)
H
lin-23(e1883)
DHB cytoplasmic:nuclear ratio
****
control(RNAi)
cki-1(RNAi)

Figure 2. CKI-1 is critical for maintaining the post-mitotic state of the AC. (A-D) Confocal images merging LAM-2::mNeonGreen with LAG-2::P2A::H2B::mTurquoise2 (left) and DHB::2xmKate2 (right) from the P6.p 4-cell stage are shown. Arrowheads indicate the position of the AC(s) in *cki-2(ok2105)* (A), *lin-35(n745)* (B), *fzr-1(ku298)* (C), and *lin-23(e1883)* (D) animals following *control(RNAi)* and *cki-1(RNAi)* treatment. Scale bars represent 5 μm. (E-H) Plots display median and IQR of DHB::2xmKate2 ratios in the AC(s) of *cki-2(ok2105)* (E), *lin-35(n745)* (F), *fzr-1(ku298)* (G), and *lin-23(e1883)* (H) animals following *control(RNAi)* and *cki-1(RNAi)* treatment (N ≥ 30 animals per treatment). Statistical significance was determined by a Mann-Whitney test ($P < 0.0001$).

700 **Table 1. Genetic analysis of negative cell cycle regulators during AC invasion.**

		% invasion		% no invasion		
Genotype	**Treatment**	**1 AC**	**≥2 AC**	**1 AC**	**≥2 AC**	**N**
wild type	*control(RNAi)*	100	0	0	0	27
rrf-3(pk1426)		97	0	3	0	30
cdc-14(he141)		100	0	0	0	35
cki-2(ok2105)		100	0	0	0	30
lin-35(n745)		100	0	0	0	31
fzr-1(ku298)		100	0	0	0	32
lin-23(e1883)		100	0	0	0	34
wild type	*cki-1(RNAi)*	100	0	0	0	29
rrf-3(pk1426)		76	9	0	15	34
cdc-14(he141)		100	0	0	0	35
cki-2(ok2105)		87	13	0	0	31
lin-35(n745)		85	12	0	3	33
fzr-1(ku298)		65	29	0	6	34
lin-23(e1883)		19	74	0	7	31

701 AC invasion was scored at the P6.p 4-cell stage of vulval development, the stage when AC
702 invasion normally occurs, using AC/VPC, BM, and cell cycle fluorescent reporters.
703
704
705
706
707
708
709
710
711
712
713
714
715
716

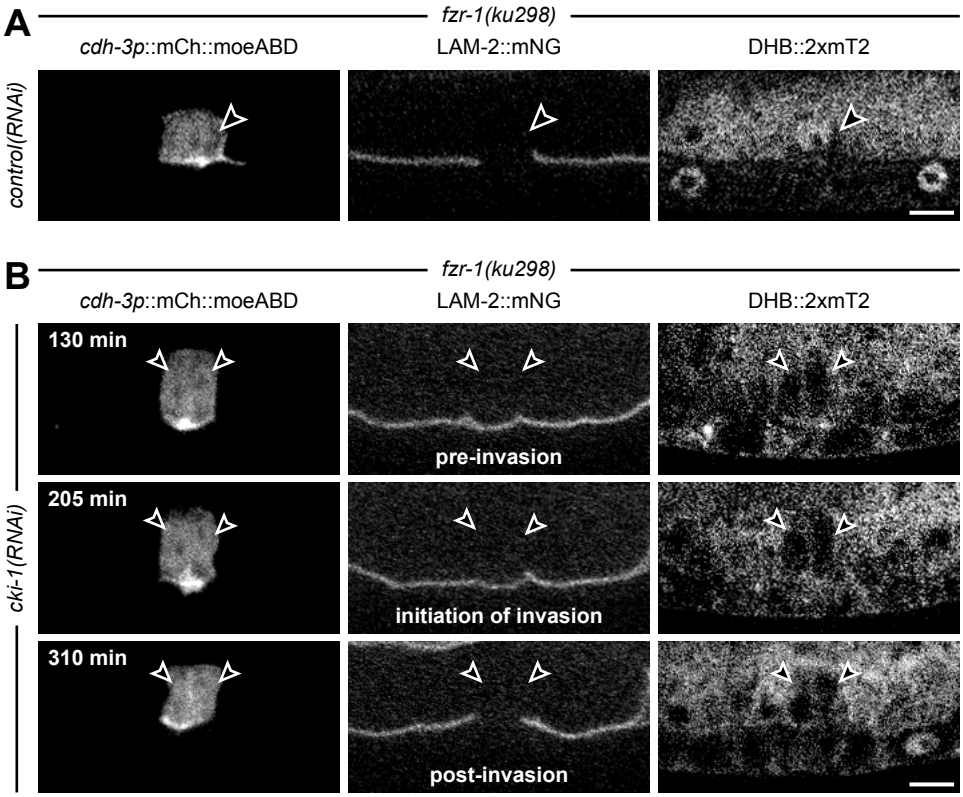
A
fzr-1(ku298)
cdh-3p::mCh::moeABD
LAM-2::mNG
DHB::2xmT2
control(RNAi)
B
fzr-1(ku298)
cdh-3p::mCh::moeABD
LAM-2::mNG
DHB::2xmT2
cki-1(RNAi)
130 min
pre-invasion
205 min
initiation of invasion
310 min
post-invasion

717 **Figure 3. Maintenance of the post-mitotic state is not required for AC invasion.** (A) Static
718 images of *cdh-3p*::mCherry::moesinABD (left), LAM-2::mNeonGreen (middle), and
719 DHB::2xmTurquoise2 (right) from the P6.p 4-cell stage are shown. Arrowheads indicate the
720 position of the AC in a *fzr-1(ku298); control(RNAi)* animal. The scale bar represents 5 μm. (B)
721 Time-lapse images of *cdh-3p*::mCherry::moesinABD (left), LAM-2::mNeonGreen (middle), and
722 DHB::2xmTurquoise2 (right) from pre-AC invasion to post-AC invasion are shown. Arrowheads
723 indicate the position of multiple invading ACs in a *fzr-1(ku298); cki-1(RNAi)* animal. The scale
724 bar represents 5 μm. See also Movie 1 and Figure S3.
725
726
727
728
729
730
731
732
733
734
735
736
737
738
739
740
741
742
743
744
745
746
747
748
749
750

751 **Movie 1. Time-lapse imaging confirms that cycling ACs can invade.** A timelapse of two
752 cycling ACs from pre-invasion to post-invasion is shown. The AC cell membrane, BM, and CDK
753 activity are visualized using an F-actin probe (*cdh-3p*::mCherry::moesinABD), an endogenous
754 *lam-2* translational reporter (LAM-2::mNeonGreen), and a ubiquitous CDK activity sensor
755 (DHB::2xmTurquoise2). The time points were acquired every 5 min for 350 min with a step size
756 of 1 μm. The scale bar represents 5 μm.
757
758
759
760
761
762
763
764
765
766
767
768
769
770
771
772
773
774
775
776
777
778
779
780
781
782
783

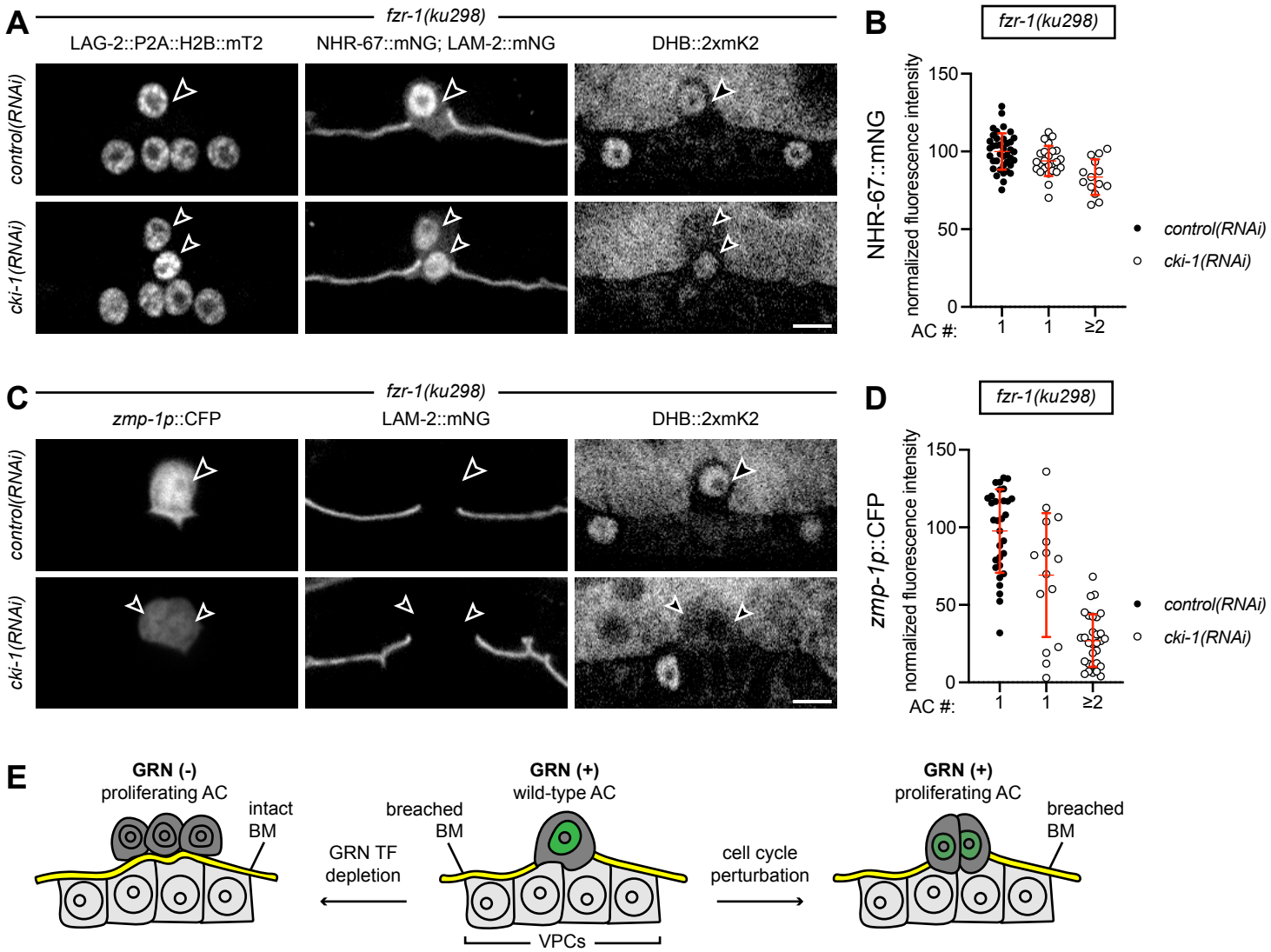
A
fzr-1(ku298)
LAG-2::P2A::H2B::mT2
NHR-67::mNG; LAM-2::mNG
DHB::2xmK2
control(RNAi)
cki-1(RNAi)
B
fzr-1(ku298)
NHR-67::mNG
normalized fluorescence intensity
150
100
50
0
AC #:
1
1
≥2
control(RNAi)
cki-1(RNAi)
C
fzr-1(ku298)
zmp-1p::CFP
LAM-2::mNG
DHB::2xmK2
control(RNAi)
cki-1(RNAi)
D
fzr-1(ku298)
zmp-1p::CFP
normalized fluorescence intensity
150
100
50
0
AC #:
1
1
≥2
control(RNAi)
cki-1(RNAi)
E
GRN (-)
proliferating AC
intact
BM
GRN TF
depletion
breached
BM
GRN (+)
wild-type AC
VPCs
cell cycle
perturbation
GRN (+)
proliferating AC
breached
BM

784 **Figure 4. Proliferating, invasive ACs retain a functionally intact pro-invasive GRN.** (A)
785 Confocal images of LAG-2::P2A::H2B::mTurquoise2 (left), NHR-67::mNeonGreen (middle),
786 LAM-2::mNeonGreen (middle), and DHB::2xmKate2 (right) from the P6.p 4-cell stage are
787 shown. Arrowheads indicate the position of the AC(s) in *fzr-1(ku298)* animals following
788 *control(RNAi)* and *cki-1(RNAi)* treatment. The scale bar represents 5 μm. (B) Plot displays mean
789 and SD of normalized NHR-67::mNeonGreen intensity in the AC(s) of *fzr-1(ku298)* animals
790 following *control(RNAi)* and *cki-1(RNAi)* treatment (N ≥ 30 animals per treatment). (C) Confocal
791 images of *zmp-1p*::CFP (left), LAM-2::mNeonGreen (middle), and DHB::2xmKate2 (right) from
792 the P6.p 4-cell stage are shown. Arrowheads indicate the position of the AC(s) in *fzr-1(ku298)*
793 animals following *control(RNAi)* and *cki-1(RNAi)* treatment. The scale bar represents 5 μm. (D)
794 Plot displays mean and SD of normalized *zmp-1p*::CFP intensity in the AC(s) of *fzr-1(ku298)*
795 animals following *control(RNAi)* and *cki-1(RNAi)* treatment (N ≥ 31 animals per treatment). (E)
796 Whereas depletion of pro-invasive GRN transcription factors (TFs) results in proliferating, non-
797 invasive ACs (left), direct perturbation of the AC cell cycle results in proliferating, invasive ACs
798 that maintain pro-invasive gene expression (right).